Supplementary Information

Prismatic alkali-ion environment suppresses plateau hysteresis in lattice oxygen redox reactions

Hao Yu[1,2,#], Ang Gao[2,#], Xiaohui Rong[2,3,*], Shipeng Shen[4], Xinqi Zheng[1], Liqin Yan[2], Haibo Wang[2], Dan Su[2], Zilin Hu[2], Wang Hay Kan[5,6], Huaican Chen[5,6], Wen Yin[5,6], Yaxiang Lu[2,7], Qinghua Zhang[2,*], Lin Gu[2], Claude Delmas[8], Liquan Chen[2,3,7], Shouguo Wang[1,9,*], Yong-Sheng Hu[2,3,7,*]

[1]School of Materials Science and Engineering, University of Science and Technology Beijing, Beijing 100083, China

[2]Key Laboratory for Renewable Energy, Beijing Key Laboratory for New Energy Materials and Devices, Laboratory for Advanced Materials & Electron Microscopy, State Key Laboratory of Magnetism, Beijing National Laboratory for Condensed Matter Physics, Institute of Physics, Chinese Academy of Sciences, College of Materials Science and Optoelectronic Technology, University of Chinese Academy of Sciences, Beijing 100190, China.

[3]Yangtze River Delta Physics Research Center Co. Ltd, Liyang 213300, China.

[4]Institute of Advanced Materials, Beijing Normal University, Beijing 100875, China.

[5]Spallation Neutron Source Science Center, Dalang, Dongguan 523000, China.

[6]Institute of High Energy Physics, Chinese Academy of Sciences, Beijing 100875, China.

[7]Huairou Division, Institute of Physics, Chinese Academy of Sciences, Beijing 101400, China.

[8]University of Bordeaux, Bordeaux INP, ICMCB UMR 5026, CNRS, Pessac 33608, France.

[9]Anhui Key Laboratory of Magnetic Functional Materials and Devices, School of Materials Science and Engineering, Anhui University, Hefei 230601, China

*Corresponding authors: Xiaohui Rong (rong@iphy.ac.cn); Qinghua Zhang (zqh@iphy.ac.cn); Shouguo Wang (sgwang@ahu.edu.cn); Yong-Sheng Hu (yshu@iphy.ac.cn)

Supplementary Notes

Supplementary Note 1. The raw material cost and average voltage of some typical Lattice Oxygen Redox (LOR) active materials are counted in Figure N1. The average charge voltage is generally higher than the average discharge voltage, indicating energy loss in the process of energy storage. The corresponding cost of the positive electrode in charge is universally lower than that in discharge. P2/P3 $Na_{0.6}Li_{0.2}Mn_{0.8}O_2$ has a high average discharge voltage owe to the maintenance of the plateau voltage in discharge. The increase of the discharge voltage is crucial for minimizing expenses and preserving energy sustainability.

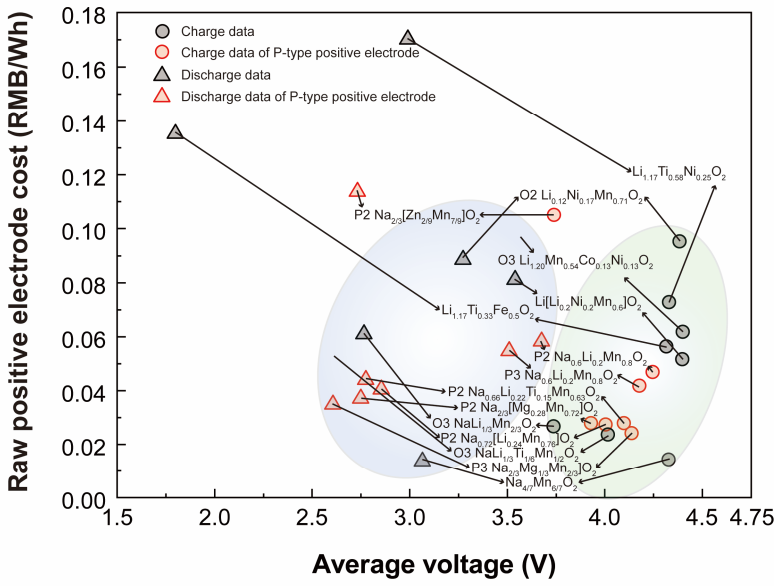

Figure N1. Average operating voltage and raw positive electrode cost of representative 3d transition metal oxide positive electrode with lattice oxygen redox reactions. The collected cut-off voltage in discharge is 2 V or 2.5 V. The circle point is the data in charge, and the triangle point represents the data in discharge. The data obtained from P-type Na-deficient transition metal oxides are represented by the red point[1-16].

Supplementary Note 2. Voltage hysteresis as a general electrochemistry behavior is usually discussed as a global system throughout the whole voltage range, however, the electrochemistry curve shown in Figure 1 in various voltage ranges and the underlying causes are diverse. For better understanding the electrochemistry behavior, further subdivision of voltage hysteresis is essential. Here, we divide voltage hysteresis in oxygen redox materials into two types plateau hysteresis and slope hysteresis without considering capacity loss and voltage fade for better controlling variables. The charge curves in Figure 1 (a)-(c) are High Voltage Plateau (HVP), and the discharge curves show HVP, slope and S shape. The second type of plateau hysteresis is shown in Figure 1 (d)-(f). The shape of the charge curve is S, and the HVP corresponds to the redox couple of O^{2-}/O_2^{n-}. The hysteresis is still obvious. As shown in Table N1, most materials belong to the type in Figure 1 (d). The last type is slope hysteresis, in which the redox couples of O^{2-}/O_2^{n-} and M^{a+}/M^{b+} are on the same slope.

Table N1 The type of voltage hysteresis and corresponding typical cathode. Each cathode belongs to one kind of figure in Figure 1.

	Hysteresis type	Typical Cathode	Corresponding figure	Ref.
1	No hysteresis	$Na_{0.6}Li_{0.2}Mn_{0.8}O_2$	Figure 1 (a)	[17]
2	Plateau hysteresis	$Na_{2/3}[Mg_{0.28}Mn_{0.72}]O_2$	Figure 1 (b)	[11]
3		$Na_{0.72}Li_{0.24}Mn_{0.76}O_2$		[13]
4		$Na_{2/3}[Mn_{7/9}Zn_{2/9}]O_2$		[2]
5		$Na_{0.66}Li_{0.22}Ti_{0.15}Mn_{0.63}O_2$		[3]
6		$Li_{1.17}Ti_{0.58}Ni_{0.25}O_2$	Figure 1 (c)	[8]
7	No hysteresis	Na_2IrO_3	Figure 1 (d)	[18]
8		$Na_2Mn_3O_7$		[12]
9	Plateau hysteresis	$Li_2Ru_{0.75}Sn_{0.25}O_3$	Figure 1 (e)	[19]
10		$Li_2Ir_{0.75}Sn_{0.25}O_3$		[20]
11		β-Li_2IrO_3		[21]
12		$Li_{1.20}Mn_{0.54}Co_{0.13}Ni_{0.13}O_2$		[6]
13		$Li[Li_{0.2}Ni_{0.2}Mn_{0.6}]O_2$		[16]
14		Na_2RuO_3		[22]
15		$Li_{1.17}Ti_{0.33}Fe_{0.5}O_2$	Figure 1 (f)	[9]
16	Slope hysteresis	$Na_2Ru_{0.75}Sn_{0.25}O_3$	Figure 1 (h)	[23]
17		$Li_{1.90}Mn_{0.95}O_{2.05}F_{0.95}$		[5]
18		$Li_{1.12-y}Ni_{0.17}Mn_{0.71}O_2$		[4]

Supplementary Figures

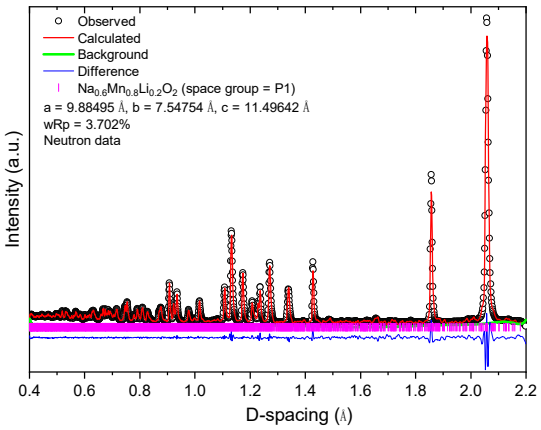

Supplementary Figure 1. Rietveld refinement of the neutron powder diffraction pattern of pristine P2-$Na_{0.6}[Li_{0.2}Mn_{0.8}]O_2$.

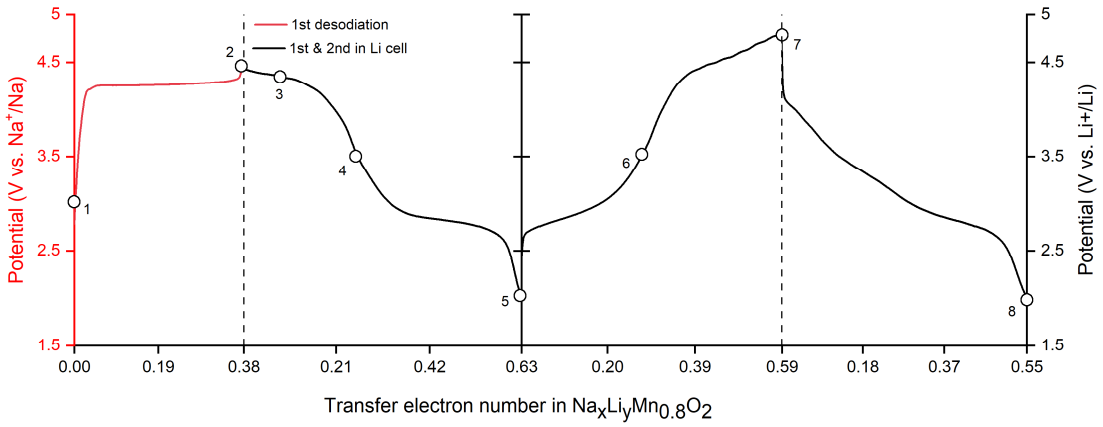

Supplementary Figure 2. Voltage curves of the desodiation and (de)lithiation of P2-NLMO. Red and black curves indicate Na and Li (de)intercalation, respectively. Points 1~8 represent the different insertion states for ex-situ characterization.

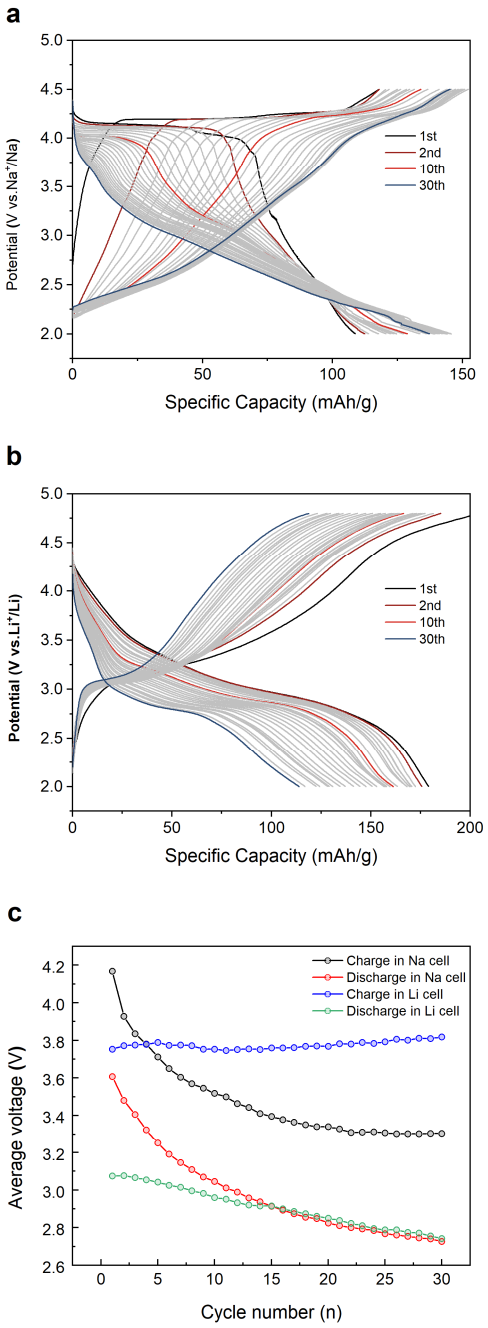

Supplementary Figure 3. Electrochemical curve for (de)sodiation or (de)lithiation of P3-NLMO. a, 30 cycles for (de)sodiation of P3-NLMO. b, 30 cycles for (de)lithiation of P3-NLMO. c, Average voltage decay of P3-NLMO in Na cell and Li cell.

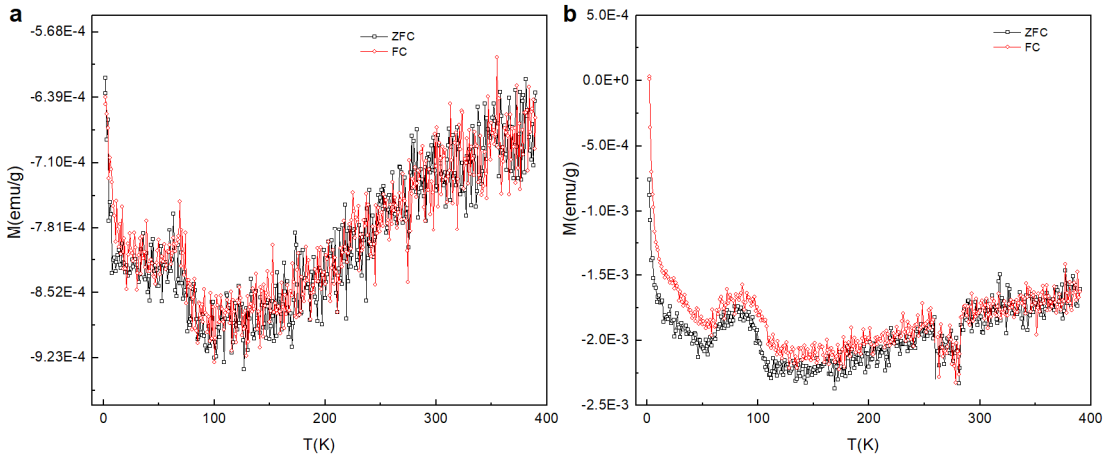

Supplementary Figure 4. Magnetic susceptibility versus temperature for the **a,** Super-P and **b,** PTFE. As the signal is poor, the signal of the copper rod is detected explaining the existence of a diamagnetic signal.

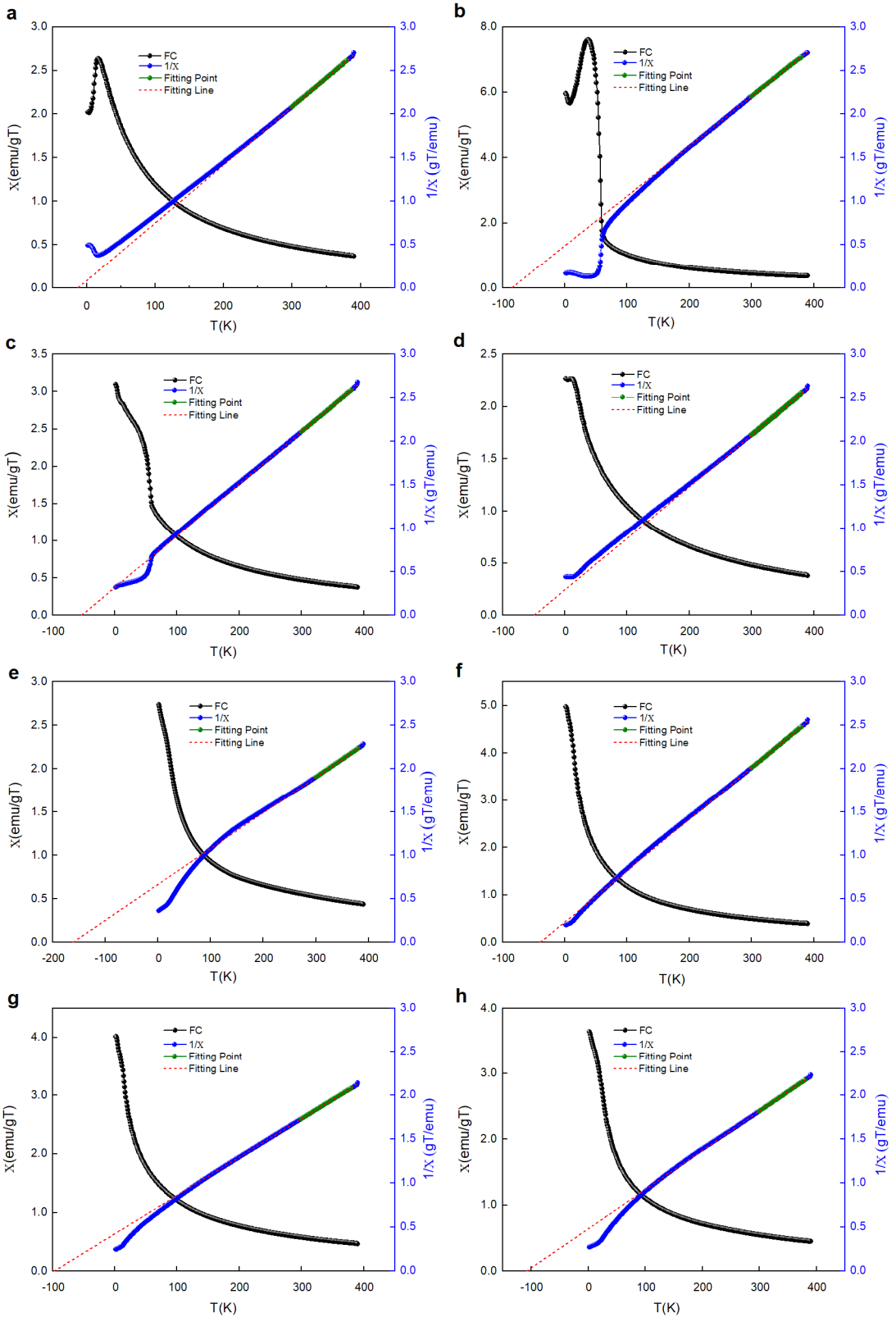

Supplementary Figure 5. Magnetic susceptibility and inverse magnetic susceptibility versus temperature for the state of P3-NLMO at Points 1-9. The red curve through the data is Curie-Weiss fitting and the green curve is the selected fitting point. The x-axis intercept of the red dotted line is the θ_{cw}.

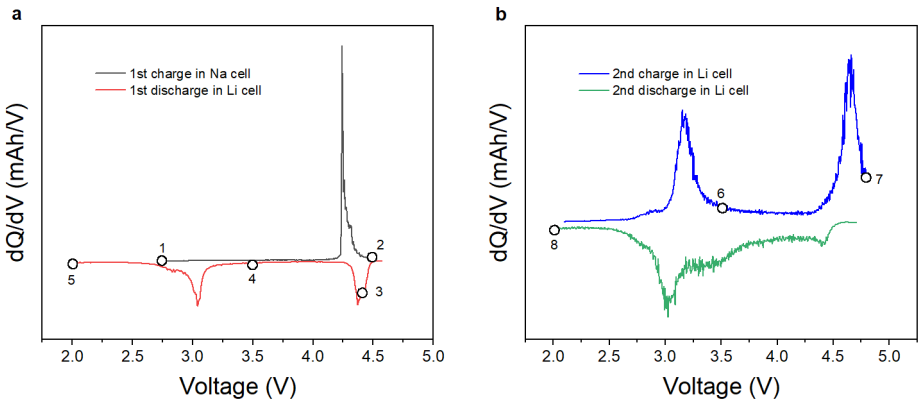

Supplementary Figure 6. dQ/dV plots for the **a,** desodiation and initial lithiation and **b,** (de)lithiation in Li and Na cells

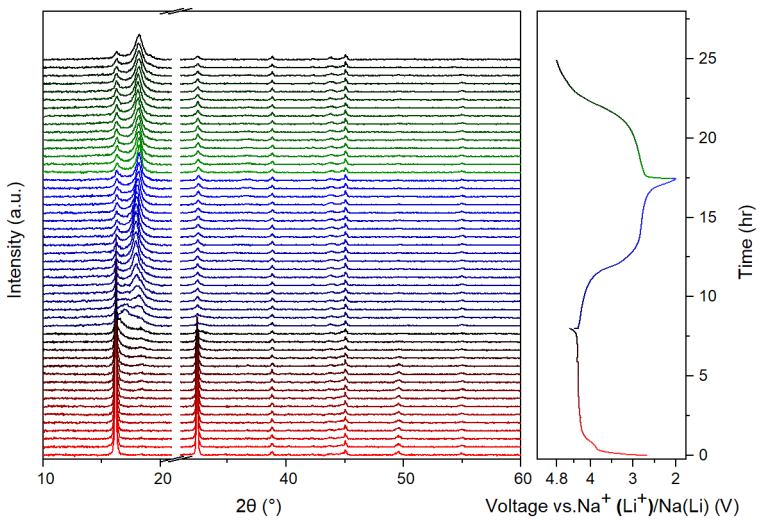

Supplementary Figure 7. The in situ XRD patterns collected during the first charge in Na cell and the first discharge and charge in Li cell for P2-NLMO.

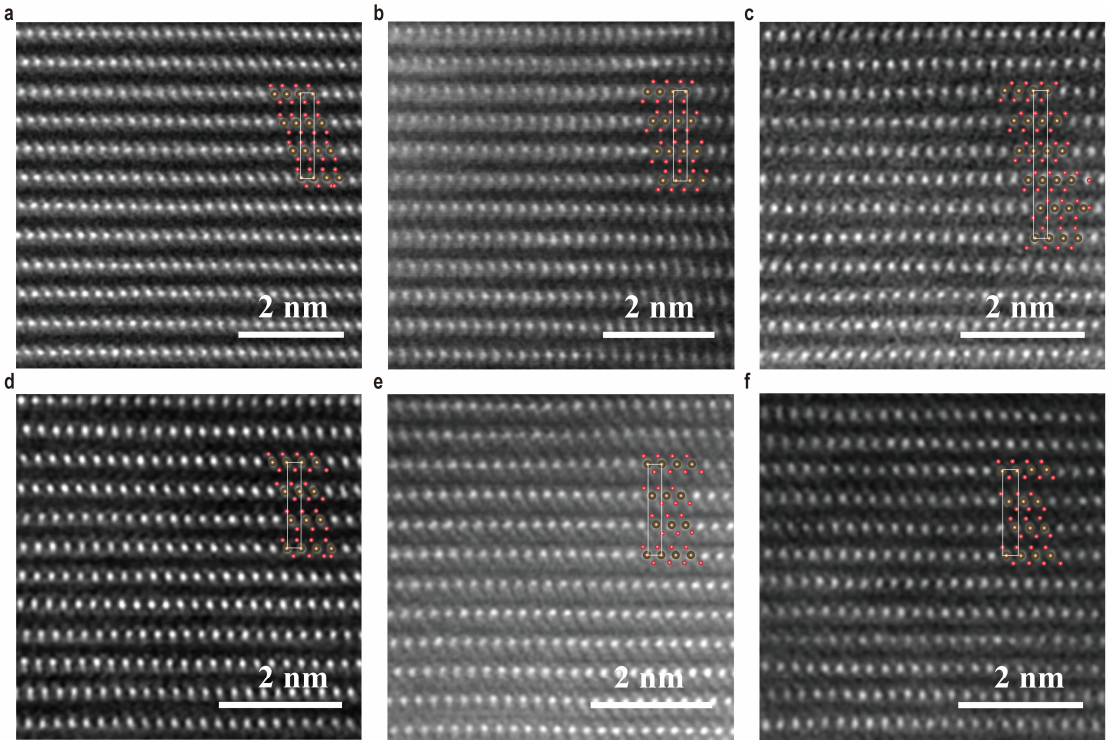

Supplementary Figure 8. High-angel annular dark-field (HAADF) images along the [100] for P3-NLMO at Point 1,2,3,4,5,7. Scale bars, 2nm.

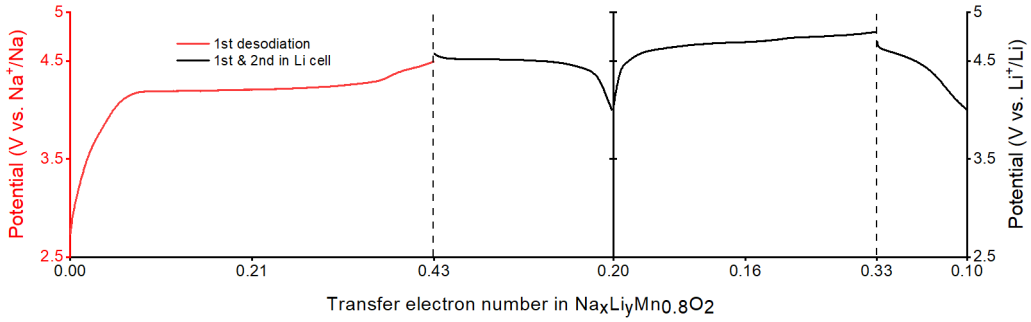

Supplementary Figure 9. Voltage curves of the desodiation and (de)lithiation of P3-NLMO between 4V and 4.8 V. Red and black curves indicate Na and Li (de)intercalation, respectively.

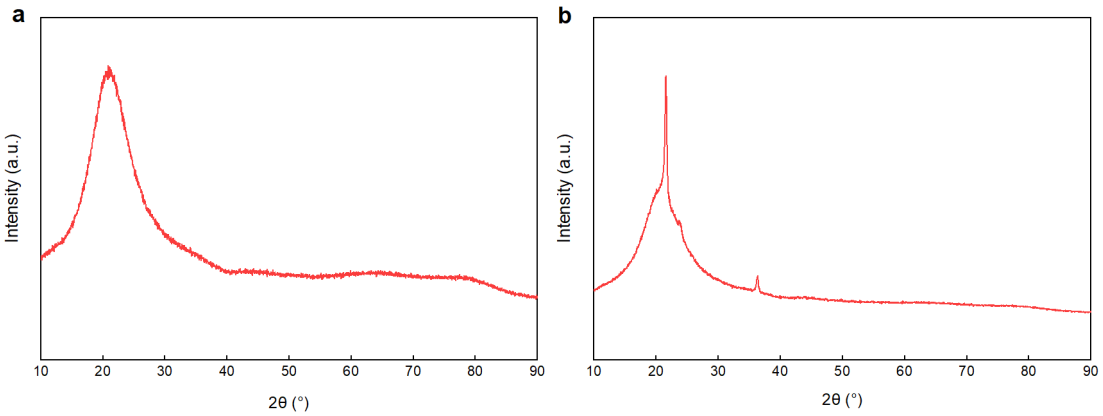

Supplementary Figure 10. a, X-ray diffraction pattern of sample holder and **b,** sample holder and plastic wraps. Revealing the amorphous wide peak from the sample holder and the sharp peaks at 21.5°, 23.8° and 36.3° from plastic wraps.

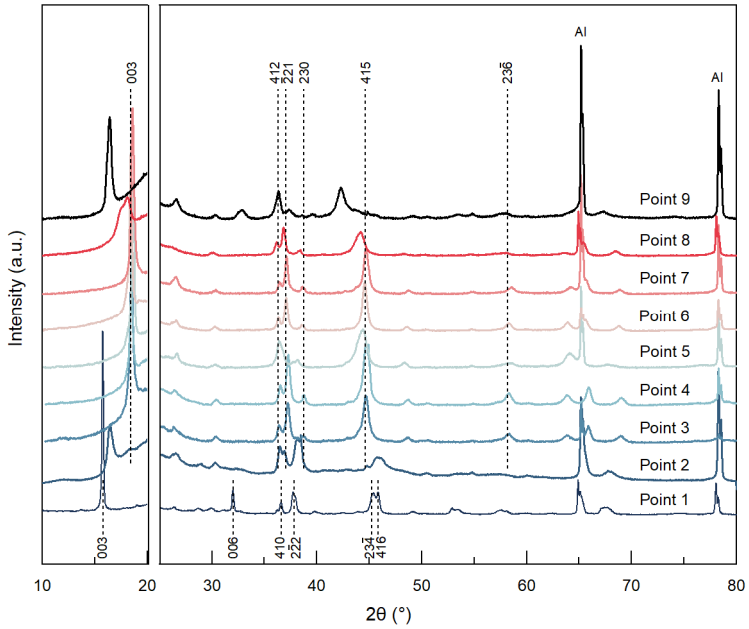

Supplementary Figure 11. The ex situ XRD patterns of P3-NLMO at different states from 10° to 80° tagged by Points 1~9.

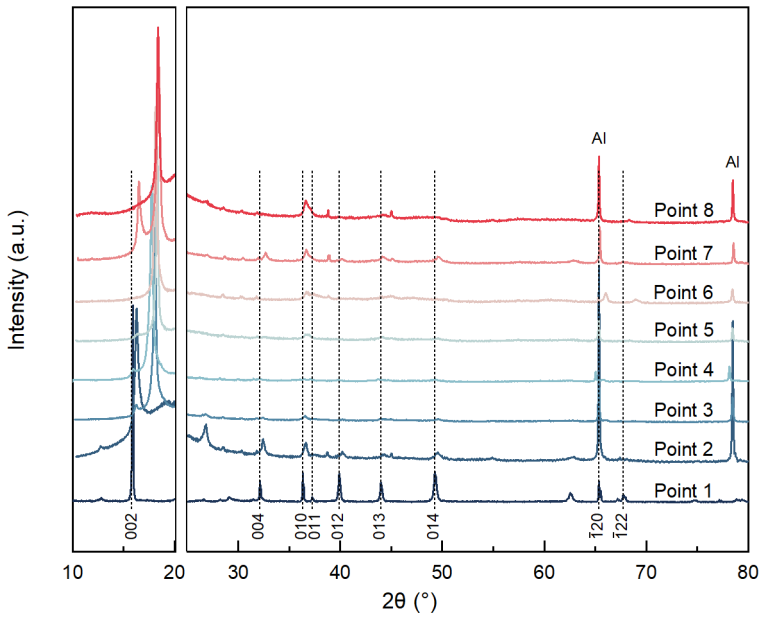

Supplementary Figure 12. The ex situ XRD patterns of P2-NLMO at different states from 10° to 80° tagged by Points 1~8.

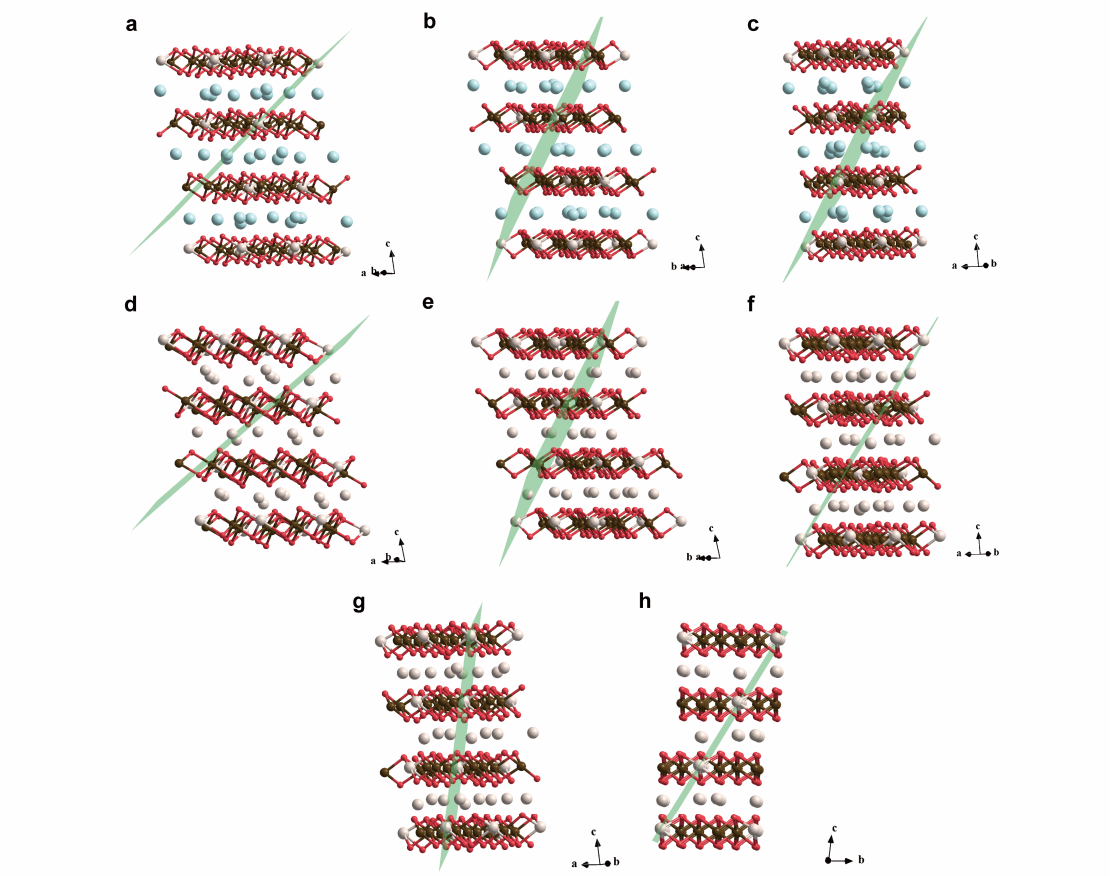

Supplementary Figure 13. a, (214) **b,** (223) and **c,** $(2\bar{1}3)$ in P3-NLMO; **d,** (214) **e,** (223) and **f,** $(2\bar{1}3)$ in O3-LLMO; **g,** $(2\bar{1}1)$ and **h**, $(02\bar{2})$ in O3-LLMO. Revealing that the (214), (223) and $(2\bar{1}3)$ crystal faces pass through alkali metal ions in the TM layer of P3-NLMO, however, not in the TM layer of O3-LLMO. Correspondingly, the alkali metal ions in the TM layer are passed through by $(2\bar{1}1)$ and $(02\bar{2})$.

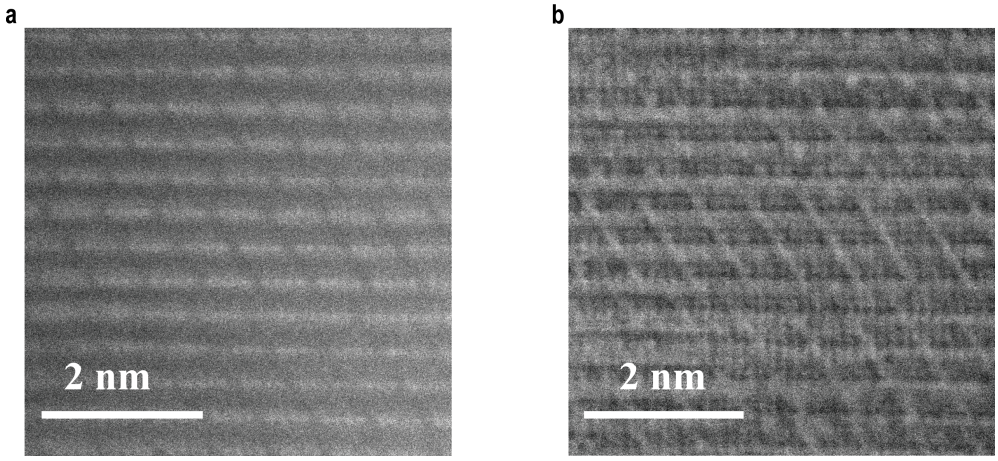

Supplementary Figure 14. a, The high-angle annular dark-field-scanning transmission electron microscope (HAADF-STEM) images and **b,** Corresponding annular bright-field (ABF)-STEM images at Point 5 (O3-$Na_{0.1}Li_x$ $[Li_{0.2}Mn_{0.8}]O_2$).

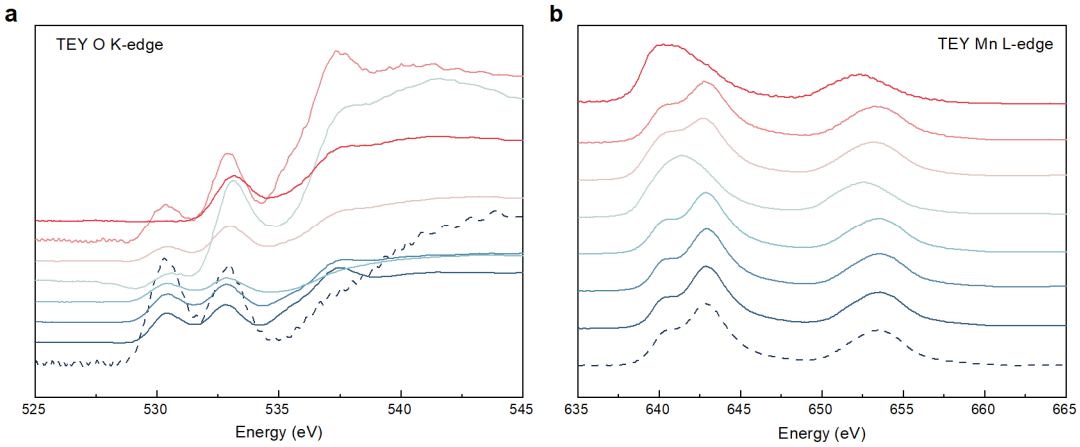

Supplementary Figure 15. Ex situ **a,** O K-edge TEY-XAS spectra and **b,** Mn $L_{2,3}$-edge TEY-XAS spectra of P2-NLMO at different states from Point 1 to Point 8.

Supplementary Tables

Supplementary Table 1. The molecular formula from ICP results, the effective moment μ_{eff} and the Curie-Weiss temperature θ_{cw} from Curie-Weiss law fit in the temperature range of 300-380 K at different SOC of P3-NLMO (Point 1-8).

Point	molecular formula	μ_{eff} (μ_B)	θ_{cw} (K)
1	$Na_{0.587}Li_{0.208}Mn_{0.8}O_2$	3.697	-13.07
2	$Na_{0.309}Li_{0.185}Mn_{0.8}O_2$	3.842	-85.55
3	$Na_{0.233}Li_{0.407}Mn_{0.8}O_2$	3.754	-53.57
4	$Na_{0.102}Li_{0.642}Mn_{0.8}O_2$	3.735	-49.47
5	$Na_{0.102}Li_{1.020}Mn_{0.8}O_2$	4.551	-161.59
6	$Na_{0.124}Li_{0.740}Mn_{0.8}O_2$	3.765	-39.52
7	$Na_{0.076}Li_{0.381}Mn_{0.8}O_2$	4.297	-97.99
8	$Na_{0.092}Li_{1.033}Mn_{0.8}O_2$	4.376	-108.38

Supplementary Table 2. The research summary of doping at alkali metal site.

Materials	Doped ion	Doped Method	Reference
$Na_xCa_yCoO_2$ ($0.45 \leqslant x \leqslant 0.64$, $0.02 \leqslant y \leqslant 0.10$)	Ca^{2+}	Dry media reaction	[24]
$Na_{0.7}Mg_{0.05}[Mn_{0.6}Ni_{0.2}Mg_{0.15}]O_2$	Mg^{2+}	Dry media reaction	[25]
$Li_{0.99}M_{0.01}Ni_{0.8}Co_{0.1}Mn_{0.1}O_2$ (M=Li, Na, K, Rb)	Li^+, Na^+, K^+, Rb^+	Dry media reaction (co-precipitation)	[26]
$(Li_{0.995}Mg_{0.005})NiO_2$	Mg^{2+}	Dry media reaction (co-precipitation)	[27]
$Li_{0.9}Mg_{0.05}CoO_2$	Mg^{2+}	Dry media reaction	[28]
$Na_{0.98}Ca_{0.01}[Ni_{0.5}Mn_{0.5}]O_2$	Ca^{2+}	Dry media reaction (co-precipitation)	[29]
$[Na_{0.67}Zn_{0.05}]Ni_{0.18}Cu_{0.1}Mn_{0.67}O_2$	Zn^{2+}	Dry media reaction (sol-gel method)	[30]
$Na_{0.67-x}Ca_xNi_{0.33}Mn_{0.67}O_{2-2x}F_{2x}$	Ca^{2+}	Dry media reaction	[31]
$Na_xK_{0.08}Ni_{0.2}Mn_{0.8}O_2$	K^+	Dry media reaction & Electrochemical intercalation reaction	[32]
$Na_{0.524}Mg_{0.146}Ni_{0.15}Fe_{0.20}Mn_{0.65}F_{0.05}O_{1.95}$	Mg^{2+}	Electrochemical intercalation reaction	[33]
$Na_{0.7}Li_{0.03}[Mg_{0.15}Li_{0.07}Mn_{0.75}]O_2$	Li^+	Dry media reaction	[34]
$LiNi_{0.95}Al_{0.04}Mg_{0.01}O_2$	Mg^{2+}	Dry media reaction (co-precipitation)	[35]
$Li_{1.1}(Ni_{0.21}Mn_{0.65}Al_{0.04})O_2$	TM	Dry media reaction & Chemical intercalation reaction	[36]
β-$A_xV_2O_5$ (A = Na, K)	Na^+, K^+	Chemical pre-intercalation	[37]

Supplementary Table 3. The ions with the same effective ion radius as the Na+ for a given coordination number[38].

Ion	Number of coordination	Effective ionic radius (ppm)
Na^{+}	6	116
Ag^{+}	6	108
Ca^{2+}	6	114
Bi^{3+}	6	117

References

1. Bai, X., Iadecola, A., Tarascon, J.-M. & Rozier, P. Decoupling the effect of vacancies and electropositive cations on the anionic redox processes in Na based P2-type layered oxides. *Energy Storage Materials* **31,** 146-155 (2020).
2. Bai, X.*, et al.* Anionic Redox Activity in a Newly Zn-Doped Sodium Layered Oxide P2-Na2/3Mn1− yZnyO2 (0< y< 0.23). *Advanced Energy Materials* **8,** 1802379 (2018).
3. Cao, X.*, et al.* Restraining oxygen loss and suppressing structural distortion in a newly Ti-substituted layered oxide P2-Na0. 66Li0. 22Ti0. 15Mn0. 63O2. *ACS Energy Letters* **4,** 2409-2417 (2019).
4. de Boisse, B. M., Jang, J., Okubo, M. & Yamada, A. Cobalt-free O2-type lithium-rich layered oxides. *Journal of The Electrochemical Society* **165,** A3630 (2018).
5. House, R. A.*, et al.* Lithium manganese oxyfluoride as a new cathode material exhibiting oxygen redox. *Energy & Environmental Science* **11,** 926-932 (2018).
6. Koga, H.*, et al.* Reversible oxygen participation to the redox processes revealed for Li1. 20Mn0. 54Co0. 13Ni0. 13O2. *Journal of The Electrochemical Society* **160,** A786 (2013).
7. Kumakura, S., Tahara, Y., Kubota, K., Chihara, K. & Komaba, S. Sodium and manganese stoichiometry of P2-type Na2/3MnO2. *Angewandte Chemie International Edition* **55,** 12760-12763 (2016).
8. Li, B.*, et al.* Capturing dynamic ligand-to-metal charge transfer with a long-lived cationic intermediate for anionic redox. *Nature Materials***,** 1-10 (2022).
9. Li, B.*, et al.* Correlating ligand-to-metal charge transfer with voltage hysteresis in a Li-rich rock-salt compound exhibiting anionic redox. *Nature Chemistry* **13,** 1070-1080 (2021).
10. Liang, X., Hwang, J. Y. & Sun, Y. K. Practical Cathodes for Sodium-Ion Batteries: Who Will Take The Crown? *Advanced Energy Materials* **13,** 2301975 (2023).
11. Maitra, U.*, et al.* Oxygen redox chemistry without excess alkali-metal ions in Na 2/3 [Mg 0.28 Mn 0.72] O 2. *Nature chemistry* **10,** 288-295 (2018).
12. Mortemard de Boisse, B.*, et al.* Highly Reversible Oxygen-Redox Chemistry at 4.1 V in Na4/7− x [□ 1/7Mn6/7] O2 (□: Mn Vacancy). *Advanced Energy Materials* **8,** 1800409 (2018).
13. Rong, X.*, et al.* Anionic redox reaction-induced high-capacity and low-strain cathode with suppressed phase transition. *Joule* **3,** 503-517 (2019).
14. Song, B.*, et al.* A novel P3-type Na 2/3 Mg 1/3 Mn 2/3 O 2 as high capacity sodium-ion cathode using reversible oxygen redox. *Journal of Materials Chemistry A* **7,** 1491-1498 (2019).
15. Wang, Q.*, et al.* Unlocking anionic redox activity in O3-type sodium 3 d layered oxides via Li substitution. *Nature materials* **20,** 353-361 (2021).
16. Zheng, J.*, et al.* Structural and chemical evolution of Li-and Mn-rich layered cathode material. *Chemistry of Materials* **27,** 1381-1390 (2015).
17. Rong, X.*, et al.* Structure-induced reversible anionic redox activity in Na layered oxide cathode. *Joule* **2,** 125-140 (2018).
18. Perez, A. J.*, et al.* Strong oxygen participation in the redox governing the structural and electrochemical properties of Na-rich layered oxide Na2IrO3. *Chemistry of Materials* **28,** 8278-8288 (2016).
19. Sathiya, M.*, et al.* Reversible anionic redox chemistry in high-capacity layered-oxide electrodes. *Nature materials* **12,** 827-835 (2013).
20. McCalla, E.*, et al.* Visualization of OO peroxo-like dimers in high-capacity layered oxides for Li-ion batteries. *Science* **350,** 1516-1521 (2015).

21. Pearce, P. E., *et al.* Evidence for anionic redox activity in a tridimensional-ordered Li-rich positive electrode β-Li_2IrO_3. *Nature materials* **16,** 580-586 (2017).
22. Mortemard de Boisse, B., *et al.* Intermediate honeycomb ordering to trigger oxygen redox chemistry in layered battery electrode. *Nature communications* **7,** 1-9 (2016).
23. Rozier, P., *et al.* Anionic redox chemistry in Na-rich Na2Ru1− ySnyO3 positive electrode material for Na-ion batteries. *Electrochemistry Communications* **53,** 29-32 (2015).
24. Han, S. C., Lim, H., Jeong, J., Ahn, D., Park, W. B., Sohn, K.-S. & Pyo, M. Ca-doped NaxCoO2 for improved cyclability in sodium ion batteries. *Journal of Power Sources* **277,** 9-16 (2015).
25. Wang, Q.-C., *et al.* Tuning P2-structured cathode material by Na-site Mg substitution for Na-ion batteries. *Journal of the American Chemical Society* **141,** 840-848 (2018).
26. He, T., *et al.* The effects of alkali metal ions with different ionic radii substituting in Li sites on the electrochemical properties of Ni-Rich cathode materials. *Journal of Power Sources* **441,** 227195 (2019).
27. Seong, W. M. & Manthiram, A. Complementary effects of Mg and Cu incorporation in stabilizing the cobalt-free LiNiO2 cathode for lithium-ion batteries. *ACS Applied Materials & Interfaces* **12,** 43653-43664 (2020).
28. Huang, Y., *et al.* Mg-pillared LiCoO2: towards stable cycling at 4.6 V. *Angewandte Chemie International Edition* **60,** 4682-4688 (2021).
29. Yu, T.-Y., Kim, J., Hwang, J.-Y., Kim, H., Han, G., Jung, H.-G. & Sun, Y.-K. High-energy O3-Na 1− 2x Ca x [Ni 0.5 Mn 0.5] O 2 cathodes for long-life sodium-ion batteries. *Journal of Materials Chemistry A* **8,** 13776-13786 (2020).
30. Peng, B., *et al.* Unusual site-selective doping in layered cathode strengthens electrostatic cohesion of alkali-metal layer for practicable sodium-ion full cell. *Advanced Materials* **34,** 2103210 (2022).
31. Mao, Q., *et al.* Mitigating the P2–O2 transition and Na+/vacancy ordering in Na 2/3 Ni 1/3 Mn 2/3 O 2 by anion/cation dual-doping for fast and stable Na+ insertion/extraction. *Journal of Materials Chemistry A* **9,** 10803-10811 (2021).
32. Wang, Y., *et al.* Pillar-beam structures prevent layered cathode materials from destructive phase transitions. *Nature Communications* **12,** 13 (2021).
33. Cui, X., *et al.* Insights into the improved cycle and rate performance by ex-situ F and in-situ Mg dual doping of layered oxide cathodes for sodium-ion batteries. *Energy Storage Materials* **45,** 1153-1164 (2022).
34. Wu, Z., *et al.* Realizing high capacity and zero strain in layered oxide cathodes via lithium dual-site substitution for sodium-ion batteries. *Journal of the American Chemical Society* **145,** 9596-9606 (2023).
35. Shen, L., *et al.* Cobalt-free nickel-rich cathode materials based on Al/Mg co-doping of LiNiO2 for lithium ion battery. *Journal of Colloid and Interface Science* **638,** 281-290 (2023).
36. Luo, D., *et al.* A Li-rich layered oxide cathode with negligible voltage decay. *Nature Energy* **8,** 1078-1087 (2023).
37. Luo, Y., *et al.* Effect of pre-intercalation on Li-ion diffusion mapped by topochemical single-crystal transformation and operando investigation. *Nature Materials***,** 1-9 (2024).
38. Shannon, R. D. Revised effective ionic radii and systematic studies of interatomic distances in halides and chalcogenides. *Acta crystallographica section A: crystal physics, diffraction, theoretical and general crystallography* **32,** 751-767 (1976).